INTERNATIONAL JOURNAL OF CLIMATOLOGY, VOL. 16, 393–403 (1996)

SIGNATURES OF A UNIVERSAL SPECTRUM FOR ATMOSPHERIC INTERANNUAL VARIABILITY IN COADS SURFACE PRESSURE TIME SERIES

A. M. SELVAM, J. S. PETHKAR, M. K. KULKARNI AND R. VIJAYAKUMAR
Indian Institute of Tropical Meteorology, Pune-411008, India

Received 27 October 1994
Accepted 17 July 1995

ABSTRACT

Annual and seasonal mean global surface pressure time series for the 25 years 1964–1988 obtained from the Comprehensive Ocean Atmosphere Data Set (COADS) were subjected to quasi-continuous periodogram spectral analysis. Periodogram estimates are summarized in the following: (i) the atmospheric interannual variability exhibits a broadband (eddy continuum) structure; (ii) the spectra follow the universal inverse power-law form of the statistical normal distribution; (ii) periodicities up to 5 years contribute to as much as 50 per cent of the total variance; (v) the high- and low-frequency El Niño–Southern Oscillation (ENSO) cycles of respective periodicities 3–4 years and 4–8 years and interdecadal oscillations are present in all the data sets.

The inverse power-law form for power spectra is ubiquitous to real-world dynamical systems and is identified as a signature of self-organized criticality or deterministic chaos.

The above results are consistent with a recently developed cell dynamical system model for atmospheric flows, which predicts self-organized criticality as intrinsic to quantum-like mechanics governing atmospheric flow dynamics. Identification of self-organized criticality in annual and seasonal mean surface pressure fluctuations and its unique quantification implies predictability of the total pattern of fluctuations. A universal spectrum for interannual variability rules out linear trends in atmospheric surface pressure patterns.

KEY WORDS: self-organized criticality; deterministic chaos; multifractals; universal spectrum for interannual variability; Comprehensive Ocean Atmosphere Data Set (COADS); surface pressure.

INTRODUCTION

The interannual variability of atmospheric flows as recorded in meteorological parameters such as wind speed, temperature, and pressure at the Earth's surface and in the atmospheric column extending up to the stratosphere have been investigated extensively, and major quasi-periodic oscillations such as the QBO (quasi-biennial oscillation) and the 3–7 years ENSO (El Niño–Southern Oscillation) cycle have been identified (Lamb, 1972; Philander, 1990; Burroughs, 1992; Chao and Philander, 1993). Such dominant cycles are, however, superimposed on an appreciable 'background noise' contributed by a continuum of eddies of all scales within the time- and space-scales investigated (Lorenz, 1990; Tsonis and Elsner, 1990; Barnett, 1991). It is important, therefore, to quantify the total pattern of fluctuations of atmospheric flows for predictability studies. Standard deterministic models for atmospheric flows based on Newtonian continuum dynamics are subject to deterministic chaos and cannot give realistic simulation and prediction of atmospheric flows (Mary Selvam, 1990; Mary Selvam *et al.*, 1992). Mary Selvam (1993a) has shown that round-off error doubles, on average, for each step of finite precision iterative computations. Round-off error will enter the mainstream computation and give unrealistic solutions in numerical weather prediction and in climate models that incorporate thousands of iterative computations in long-term numerical integration schemes. Realistic simulation therefore requires alternative non-deterministic models that can predict the observed non-linear variability of atmospheric flows. Long-range spatio-temporal correlations are intrinsic to atmospheric flows and are manifested as the self-similar fractal geometry to the global cloud cover pattern and the inverse power-law form for atmospheric eddy energy spectrum documented by Lovejoy and

CCC 0899-8418/96/040393-11

Schertzer (1986) and Tessier *et al.* (1993). Geophysical phenomena, in general, exhibit inverse power-law form for power spectra (Agnew, 1992), indicating self-similar (fractal) fluctuations in time. Traditional meteorological theory cannot explain satisfactorily the observed self-similar space–time structure of atmospheric flows (Tessier *et al.*, 1993). Such long-range non-local connections are ubiquitous to real-world dynamical systems and are now identified as the signatures of self-organized criticality (Bak *et al.*, 1988). The physics of self-organized criticality is not yet identified. In this paper a cell dynamical system model for atmospheric flows (Mary Selvam, 1990; Mary Selvam *et al.*, 1992; Mary Selvam, 1993b; Selvam and Radhamani, 1994; Selvam and Joshi, 1995) is summarized. The model predicts self-organized criticality as intrinsic to quantum-like mechanics governing atmospheric flows, and as a natural consequence leads to the result that the atmospheric eddy energy spectrum represents the statistical normal distribution. The model predictions are in agreement with continuous periodogram analyses of 25 years (1964–1988) annual and seasonal mean oceanic surface pressure (COADS, 1985) for (i) 26 grid-points representative of diverse global climatic regimes and (ii) all available grid-points in the Northern and Southern Hemispheres for one representative season, September to November. Such unique quantification for the inverse power-law form of the atmospheric eddy energy spectrum implies predictability of the total pattern of atmospheric fluctuations.

A brief introduction to the concept of 'fractals' is given first, followed by the application of cell dynamical model concepts for the prediction of interannual variability of atmospheric flows.

MULTIFRACTAL STRUCTURE OF SPACE-TIME FLUCTUATIONS

Non-linear dynamical systems in nature, such as atmospheric flows, exhibit complex spatial patterns, e.g. cloud geometry, that lack a characteristic (single) length-scale concomitant with temporal fluctuations that lack a single time-scale. The mathematical concept of 'fractals' introduced by Mandelbrot (1977) provides powerful tools for describing and quantifying the universal symmetry of self-similarity (Schroeder, 1991) underlying the seemingly irregular complex geometrical shapes and temporal fluctuations.

2.1. Fractal geometry

Objects in nature are self-similar fractals, i.e. the internal small-scale structure resembles the whole object in shape. The fractal dimension D of such a self-similar object is given as

$$D = \frac{\mathrm{d}\ln M}{\mathrm{d}\ln R}$$

where M is the mass contained within a distance R from a point in the extended object. A graph of M versus R on logarithmic scale will give a straight line of negative slope D, i.e. the graph exhibits inverse power-law form indicating long-range spatial correlations. Constant value for D indicates logarithmic stretching over the length-scale R. Objects in nature exhibit multifractal structure, i.e. the fractal dimension D varies with length-scale R range. The region of constant fractal dimension D is associated with scale invariance, namely, the large- and small-scale structures are related to each other by the scale ratio only, independent of the details of the nature of growth.

2.2. Fractals in time

Spatially extended fractal objects in nature support fluctuations of dynamical processes on all time-scales. The power spectra of such broadband fluctuations exhibit an inverse power-law of form $1/f^{\alpha}$, where f is the frequency and α the exponent. In general α decreases with f and approaches 1 for low frequencies. Such spectra, described as $1/f$ or $1/f$-like spectra of temporal fluctuations are ubiquitous to dynamical systems in nature (West and Shlesinger, 1989). The frequency range over which α is constant therefore exhibits self-similarity or scale invariance in temporal fluctuations, i.e. the fluctuations are fractals in time. The intensity or variance of longer and shorter period fluctuations are mutually related by a scale factor alone, independent of the nature of dynamical processes. The fluctuations exhibit long-range temporal correlations. Also, temporal fluctuations exhibit multifractal structure because α varies for different ranges of frequency f. $1/f$ power-law would seem natural, and white noise (flat distribution) would be the subject of involved investigation (West and Shlesinger, 1989).

2.3. *Self-organized criticality: space–time fractals*

Until very recently (1988), fractal geometry to the spatial pattern and fractal fluctuations in time of dynamical processes of the same extended dynamical system were treated as two disparate multidisciplinary fields of research (Bak and Chen, 1989). The long-range spatio-temporal correlations underlying spatial and temporal power-law behaviour of dynamical systems was identified as a unified manifestation of self-organized criticality in 1988 (Bak *et al.*, 1988).

The unifying concept of self-organized criticality underlying fractals, self-similar scaling, broadband frequency spectra, and inverse power-law distributions offers a new and powerful means of describing certain basic aspects of spatial form and dynamical (temporal) processes of a dynamical system. The systems in which self-organized criticality is observed range from the physical to the biological to the social. Rapid advances in applications of these new concepts have been made, particularly in the field of physiology and medicine (Goldberger *et al.*, 1990; Skinner, 1994). It is now recognized that fractal architecture to the spatial pattern serves as robust, stable structures for the regulation and maintenance of vital functions of lungs, heart, liver, kidneys, brain, etc. (West, 1990). Self-similar fractal growth pattern in the plant kingdom gives rise to the observed beautiful phyllotactic patterns, i.e. the elaborate patterns of fruits in the sunflower capitulum, florets in the capitulum of daisy, scales on a pineapple and on a pinecone, etc. (Jean, 1994). Phyllotactic patterns incorporate with mathematical precision the fibonacci mathematical series (Stewart, 1995), where each term is the sum of two previous terms and the ratio of each term to the previous term approaches the golden mean $\tau = (1 + \sqrt{5})/2 = 1{\cdot}618$. Such patterns, although pleasing to the eye, combine maximum packing efficiency while preserving the shape for different sizes of a particular species, such as daisy flowers of different sizes.

CELL DYNAMICAL SYSTEM MODEL

In summary (Mary Selvam, 1990; Mary Selvam *et al.*, 1992) the model is based on the concept of Townsend (1956) that atmospheric large eddy circulations form by spatial integration of enclosed turbulent eddies. The energy (kinetic) of successively larger eddy circulations therefore follows the statistical normal distribution characteristics according to the Central Limit Theorem. Therefore the square of the eddy amplitude represents the eddy probability density. Such a result, that the additive amplitudes of eddies when squared represent the probability densities, governs subatomic dynamics of quantum systems. Atmospheric flows therefore follow quantum-like mechanical laws. The model also predicts the logarithmic wind profile relationship for atmospheric flows. The overall envelope of the large eddy traces a logarithmic spiral with the quasi-periodic Penrose tiling pattern for the internal structure. Atmospheric circulation structure therefore consists of a nested continuum of vortex roll circulations (vortices within vortices) with a two-way ordered energy flow between the larger and smaller scales. Such a concept is in agreement with the observed long-range spatio-temporal correlations in atmospheric flow pattern. Power spectral analysis will resolve such logarithmic spiral flow structure as a continuum of eddies with embedded dominant wavebands with peak periodicities P_n given as

$$P_n = T(2 + \tau)\tau^n \tag{1}$$

where τ is the golden mean equal to $(1 + \sqrt{5})/2$ $(= 1{\cdot}618)$, n is an integer ranging from positive to negative values including zero, and T is the primary perturbation time period equal to the annual (summer to winter) cycle of solar heating in the present study.

The conventional power spectrum plotted as the percentage contribution to total variance versus the frequency (period) in log–log scale will now represent the eddy probability density on logarithmic scale versus the standard deviation of the eddy fluctuations on linear scale because the logarithm of the eddy wavelength represents the standard deviation, i.e., the root-mean-square (r.m.s.) value of eddy fluctuations. This follows from the concept of logarithmic wind profile and also that the r.m.s. value of eddy fluctuations at each stage forms the mean level for the next stage of eddy growth. The r.m.s. value of the eddy fluctuations can be represented in terms of statistical normal distribution as follows. A normalized standard deviation $t = 0$ corresponds to cumulative percentage probability density equal to 50 for the mean value of the distribution. Because the logarithm of the wavelength

represents the r.m.s. value of eddy fluctuations, the normalized standard deviation t is defined for the eddy energy spectrum as

$$t = (\log L/\log T_{50}) - 1 \tag{2}$$

where L is the period in years and T_{50} is the period up to which the cumulative percentage contribution to total variance is equal to 50 and $t=0$. Log T_{50} also represents the mean value for the r.m.s. eddy fluctuations and is consistent with the concept of the mean level represented by r.m.s. eddy fluctuations. In the following section it is shown that continuous periodogram analyses of global annual and seasonal mean surface pressure for the 25-year period 1964–1988 are in agreement with model predictions.

DATA AND ANALYSIS

The annual (January–December) and the seasonal means for the four seasons DJF (December–February), MAM (March–May), JJA (June–August), and SON (September–November) for 26 grid-points representative of diverse global climatic regimes for the 25-year period (1964–1988) was taken from the Comprehensive Ocean Atmosphere Data Set (COADS, 1985).

Also, all available grid-points numbering 1590 and 153 respectively in the Northern and Southern Hemispheres for one representative season, namely, September to November, for the above period of study was used for the analysis.

The broadband power spectrum of the surface pressure time series can be computed accurately by an elementary but very powerful method of analysis developed by Jenkinson (1977), which provides a quasi-continuous form of the classical periodogram allowing systematic allocation of the total variance and degrees of freedom of the data series to logarithmically spaced elements of the frequency range (0·5,0). The periodogram is constructed for a fixed set of 10 000(m) periodicities, which increase geometrically as $L_m=2\exp(Cm)$, where $C=0{\cdot}001$ and $m=0, 1, 2, \ldots, m$. The data series Y_t for the N data points was used. The periodogram estimates the set of $A_m\cos(2\pi\nu_m t-\phi_m)$, where A_m, ν_m, and ϕ_m denote, respectively, the amplitude, frequency, and phase angle for the mth periodicity. The cumulative percentage contribution to total variance was computed starting from the high-

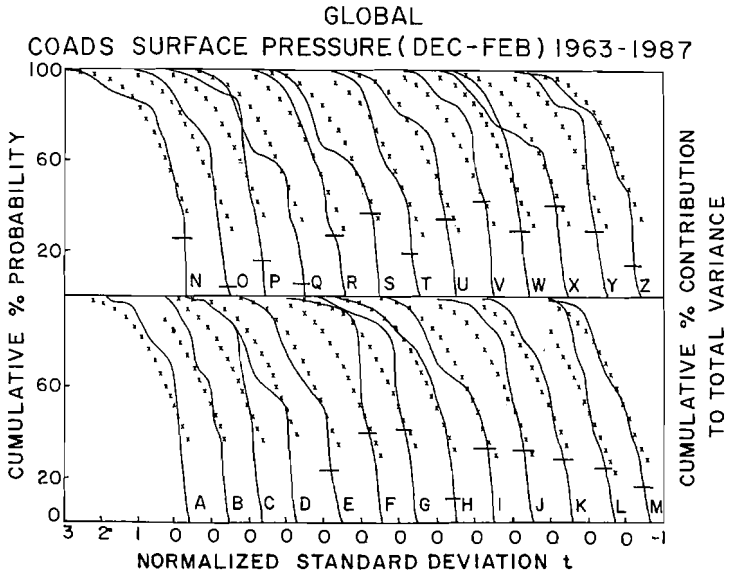

Figure 1. Power spectra of 25 years (1963–1987) seasonal (December–February) mean surface pressure time series for 26 globally representative grid-points

frequency side of the spectrum. The period T_{50} at which 50 per cent contribution to total variance occurs is taken as reference and the normalized standard deviation t_m values are computed as (equation 2)

$$t_m = [(\log L_m; \log T_{50}) - 1]$$

The cumulative percentage contribution to total variance and the corresponding t values are plotted as continuous lines in Figures 1–5 for seasonal (DJF, MAM, JJA, SON) and annual means of COADS surface pressure for the 26 globally representative grid-points for the 25-year period 1964–1988. The cumulative normal probability density distribution corresponding to the normalized standard deviation t values are shown as crosses in

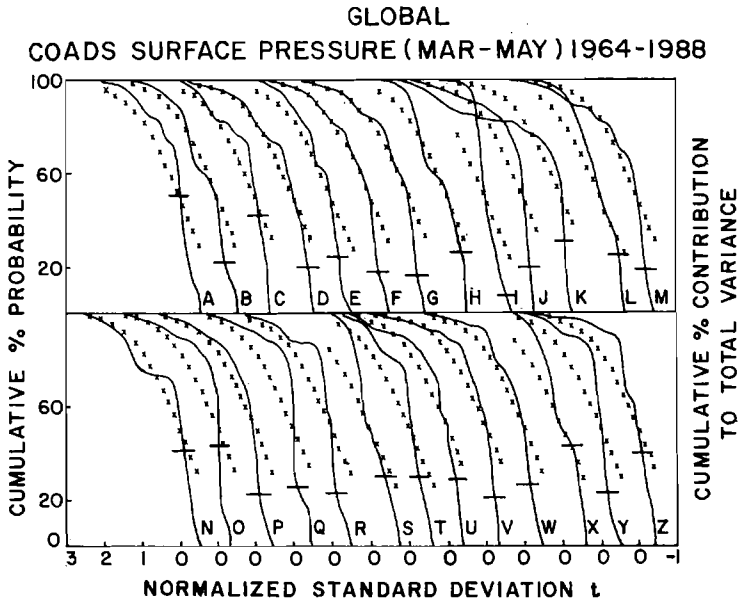

Figure 2. Power spectra of 25 years (1964–1988) seasonal (March–May) mean surface pressure time series for 26 globally representative grid-points

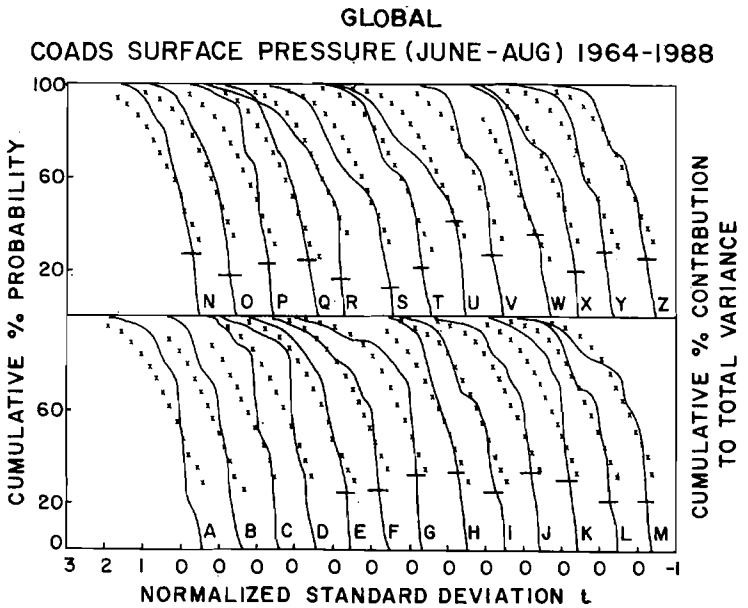

Figure 3. Same as Figure 2 but for June–August

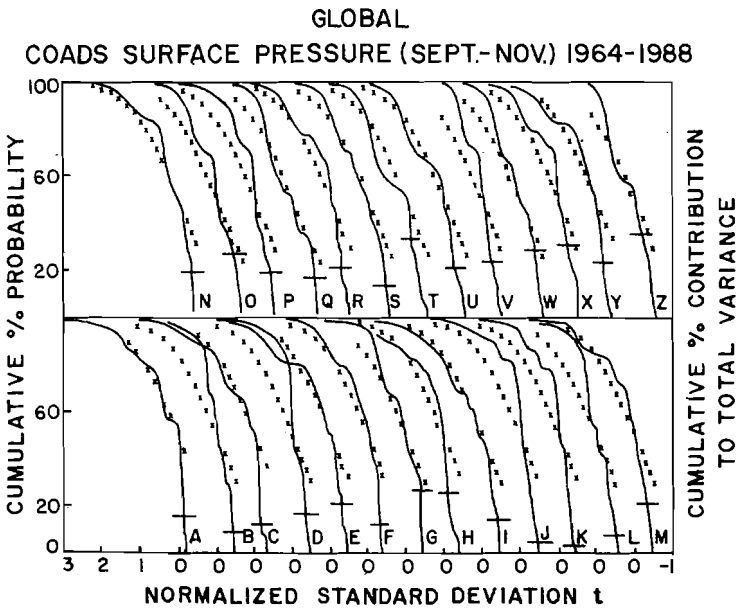

Figure 4. Same as Figure 2 but for September–November

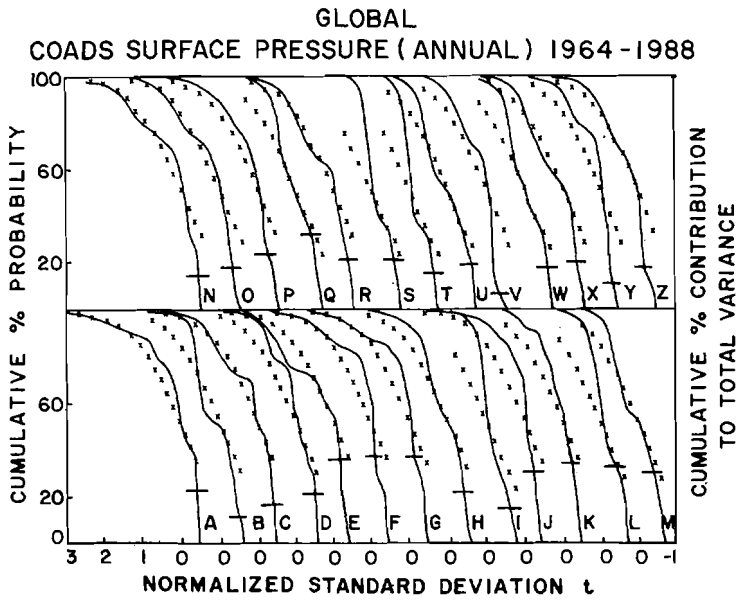

Figure 5. Same as Figure 2 but for the annual mean

Figures 1–5. It is seen that the cumulative percentage contribution to total variance closely follows the cumulative normal probability density distribution. The 'goodness of fit' was tested using the standard statistical χ^2 test (Spiegel, 1961). The horizontal lines in the lower part of Figures 1–5 indicate the lower limit above which the fit is good at the 95 per cent level of significance.

It is seen that almost all spectra exhibit local deviations from a normal distribution. Such deviations may arise from dominant wavebands (equation 1) embedded in the eddy continuum. It is possible that the fractal dimension in different wavebands may differ from that corresponding to the model predicted statistical normal distribution for the eddy continuum as a whole.

Table I gives the following periodogram estimates corresponding to Figures 1–5: (i) the mean and standard deviation of the data series; (ii) the atmospheric eddies of periodicities up to T_{50} that contribute to 50 per cent of the

Table I

Spectrum	Latitude (°N)	Longitude (°E)	Season	Mean (mb)	SD (mb)	T_{50} (years)	Periodicities (years) contributing to maximum normalized variance (H) in the waveband, with $H \geqslant 1{\cdot}0$						
A	50	178	DJF	999·3	4·5	3·2	2·1	2·7	3·3	11·1			
			MAM	1008·6	4·3	4·8	2·2	3·0	3·7	4·9	10·6		
			JJA	1012·2	1·8	4·5	2·2	4·1	5·5	11·3			
			SON	1008·0	3·2	2·4	2·2	3·6	5·9	8·7			
			ANN	1007·0	1·7	3·4	2·3	3·5	4·2	8·7			
B	50	318	DJF	1003·6	4·7	3·7	2·0	2·3	2·6	3·8	7·3	12·2	
			MAM	1010·9	3·7	4·3	2·0	4·0	5·8	13·1			
			JJA	1014·5	1·8	6·0	3·1	3·8	6·9	21·7			
			SON	1010·8	3·4	3·7	2·2	3·0	4·0	5·3			
			ANN	1010·0	1·7	4·6	2·0	2·8	3·4	12·0			
C	54	350	DJF	1009·5	5·0	2·9	2·0	2·8	3·2	3·9			
			MAM	1012·7	3·5	3·3	2·2	2·8	3·5	15·9			
			JJA	1014·9	2·7	6·2	2·5	2·9	3·4	7·2	23·9		
			SON	1010·4	3·9	2·7	2·1	2·5	3·4	6·5	17·6		
			ANN	1011·9	1·8	3·4	2·0	2·3	2·8	4·0	16·1		
D	42	308	DJF	1012·7	3·2	2·8	2·3	2·6	7·9				
			MAM*	1014·7	2·3	3·8	2·0	2·5	3·1	3·9	5·0	14·2	
			JJA	1019·0	1·4	4·7	2·1	3·1	3·7	4·5	5·9		
			SON	1017·4	1·8	3·9	2·2	2·5	3·0	4·1	5·6		
			ANN	1016·0	1·2	4·1	2·0	2·4	3·1	4·1	5·4	13·6	
E	42	178	DJF	1003·5	5·7	3·8	2·7	3·3	10·4	21·7			
			MAM	1014·3	3·3	5·2	3·5	4·5	10·6				
			JJA	1015·9	1·6	3·9	2·3	3·9	6·1	16·9			
			SON	1015·0	2·1	3·3	2·0	2·4	2·8	4·2	5·7		
			ANN	1012·2	1·7	3·7	3·3	5·1					
F	−22	148	DJF	1009·3	1·6	4·2	2·4	2·9	3·6	4·7	6·5		
			MAM	1013·8	1·0	3·7	3·0	3·5	4·9	7·1	20·5		
			JJA	1017·7	1·2	3·5	2·7	3·3	6·0	19·6			
			SON	1014·6	1·5	3·4	2·4	3·1	3·5	4·3	5·4	14·5	
			ANN	1013·8	0·9	3·5	2·4	3·5	4·4	22·9			
G	−24	150	DJF	1010·3	1·4	3·7	2·1	2·8	3·5	4·7			
			MAM	1014·5	1·2	3·6	2·9	3·5	7·2				
			JJA	1018·3	1·4	3·4	2·7	3·5	5·4	9·1			
			SON	1015·3	1·5	4·4	2·4	2·4	4·4	13·9			
			ANN	1014·6	1·0	3·5	2·4	3·5	4·4				
H	−22	320	DJF	1013·2	1·0	3·9	2·0	2·3	2·7	4·0	4·9	6·6	9·3
			MAM	1015·0	0·6	4·1	2·0	3·3	4·4	12·4			
			JJA	1019·6	1·2	4·3	2·2	2·5	2·9	3·5	4·3	6·7	11·1
			SON	1015·9	0·9	3·2	2·1	3·1	3·8	4·8	11·3		
			ANN	1015·9	0·5	4·4	2·0	2·2	2·5	3·0	6·5	10·4	
I	−28	6	DJF	1017·5	1·0	4·1	2·1	2·3	2·9	3·4	4·2		
			MAM	1018·4	0·9	11·9	4·8	15·8					
			JJA	1022·1	0·8	4·1	2·2	4·0	5·5	16·8			
			SON	1021·1	1·1	3·6	2·1	2·4	2·7	4·4	6·0	12·2	
			ANN	1019·8	0·6	14·1	4·2	23·5					
J	−40	140	DJF	1014·2	1·2	4·1	2·0	2·5	3·0	4·3	5·6	7·9	14·3
			MAM	1017·7	1·9	2·9	2·6	3·0	4·2				
			JJA	1016·6	3·0	3·2	2·2	2·7	3·3	5·4	10·1		
			SON	1014·8	2·6	3·7	2·2	2·5	3·0	4·0	8·0		
			ANN	1015·8	1·4	3·1	2·0	2·2	2·6	3·1	5·4	9·3	
K	−40	148	DJF	1013·4	1·3	5·1	2·4	4·1	5·3	7·3	23·9		
			MAM	1017·7	1·7	2·5	2·3	3·0	13·9				
			JJA	1017·7	2·8	3·3	2·2	2·5	2·7	3·4	5·2	7·2	
			SON	1014·3	2·4	3·7	2·5	3·0	4·0	8·1	13·7		
			ANN	1015·8	1·2	3·3	2·0	2·2	2·5	3·3	4·1	5·2	7·3 13·4

Continued

Table I. 'Continued'

Spectrum	Latitude (°N)	Longitude (°E)	Season	Mean (mb)	SD (mb)	T_{50} (years)	Periodicities (years) contributing to maximum normalized variance (H) in the waveband, with $H \geqslant 1{\cdot}0$							
L	−36	24	DJF	1013·8	0·9	8·5	2·0	2·7	4·6	9·4	21·7			
			MAM	1016·3	1·1	7·0	2·1	2·4	2·9	4·7				
			JJA	1019·7	1·1	3·7	2·1	2·9	3·9	14·0				
			SON	1017·3	0·9	5·1	2·1	2·4	2·8	3·3	5·3	7·6	13·0	
			ANN	1016·8	0·7	7·7	2·1	2·8	4·8	8·5				
M	18	110	DJF	1016·7	1·3	6·1	2·0	3·3	6·0	12·1				
			MAM	1011·2	0·9	3·3	2·0	2·3	2·6	3·5	6·0	12·7		
			JJA	1005·5	1·1	3·5	2·4	2·9	3·6	5·7				
			SON	1011·3	1·0	3·8	2·3	2·9	3·7	4·9	8·4			
			ANN	1011·2	0·7	8·1	2·0	3·2	4·7	6·0	8·6			
N	18	134	DJF	1014·9	1·0	2·9	2·3	2·9	3·3	3·8	4·8	25·0		
			MAM	1013·6	1·0	4·3	2·9	3·5	4·4					
			JJA	1009·3	1·1	3·7	2·4	2·7	3·7	4·5	6·1	10·7		
			SON	1010·5	0·9	4·2	2·5	3·2	7·6					
			ANN	1012·0	0·6	4·2	2·4	3·5	4·4	5·9				
O	12	54	DJF	1015·0	0·7	4·4	2·7	3·2	4·7	22·8				
			MAM	1011·3	0·5	3·6	2·6	3·6	4·6					
			JJA	1005·5	0·7	3·6	2·2	2·4	2·7	3·5	4·2	5·9	8·7	14·2
			SON	1011·6	0·7	7·0	2·1	2·4	2·7	7·4				
			ANN	1010·9	0·4	4·5	2·7	3·6	4·5	6·5				
P	14	128	DJF	1012·7	1·1	3·4	2·1	2·3	2·9	3·4	4·6			
			MAM	1011·9	0·8	3·7	2·8	3·4	4·7	6·8	11·2			
			JJA	1008·5	0·8	3·5	2·4	2·8	3·6	4·5	6·0			
			SON	1009·6	0·9	4·7	2·4	3·5	4·9	11·5				
			ANN	1010·7	0·5	4·0	2·4	3·5	4·3	5·3	11·3			
Q	10	54	DJF	1014·1	0·5	4·3	2·7	4·0						
			MAM	1011·2	0·4	3·5	2·2	3·5						
			JJA	1007·2	0·7	5·7	2·4	2·7	3·1	3·5	4·3	5·9	8·5	
			SON*	1011·7	0·6	7·8	2·1	2·5	3·0	7·5	13·0			
			ANN	1011·1	0·4	9·7	2·6	3·0	3·5	8·1	12·9			
R	6	80	DJF	1010·9	0·7	4·9	2·4	4·7	6·5	19·5				
			MAM	1009·1	0·7	3·9	2·2	3·7	5·2	23·4				
			JJA	1008·1	0·5	2·6	2·2	4·1	8·9					
			SON	1009·6	0·7	4·4	2·2	2·4	3·0	3·6	4·8	8·7		
			ANN	1009·5	0·4	4·6	2·2	3·6	4·8					
S	−6	46	DJF	1011·4	0·6	4·2	2·0	2·6	4·0	5·9				
			MAM	1011·2	0·6	11·5	2·1	4·5	6·3	9·9				
			JJA	1014·3	0·6	4·3	2·1	2·6	2·9	3·6				
			SON	1013·2	0·9	6·1	2·6	3·1	3·7	5·7	7·9	12·1		
			ANN	1012·5	0·5	22·2	2·6	3·0	3·6	4·4	5·7			
T	−16	40	DJF	1010·4	0·7	6·7	4·2	6·5						
			MAM	1013·1	0·5	6·0	2·2	2·5	3·9	4·7	6·8			
			JJA	1018·2	0·6	4·5	2·1	2·6	3·0	3·5	4·2	5·4	22·8	
			SON	1015·1	0·5	5·6	3·1	3·7	4·6					
			ANN	1014·2	0·4	21·6	3·4	4·3						
U	−26	34	DJF	1012·5	1·0	4·2	2·1	2·7	3·3	4·5				
			MAM	1016·6	0·7	3·0	2·2	2·6	3·0	3·9	4·8	6·1	8·5	
			JJA	1021·8	1·0	3·3	2·2	2·5	3·2	6·0				
			SON	1017·4	0·7	5·0	2·1	3·2	3·9	5·2				
			ANN	1017·1	0·6	7·8	2·1	2·6	3·0	4·7	8·3			
V	−26	110	DJF	1010·3	1·4	4·2	2·1	2·6	3·1	4·6	6·1	24·0		
			MAM	1014·6	0·9	2·8	2·2	2·5	3·0	3·5	5·1	15·2		
			JJA	1018·0	1·3	3·5	2·2	2·6	3·3	4·2	10·7			
			SON	1015·8	1·0	4·5	2·4	3·0	3·6	4·8	10·6			
			ANN	1014·7	0·7	3·9	3·5	4·3	12·3					

Continued

Table I. 'Continued'

Spectrum	Latitude (°N)	Longitude (°E)	Season	Mean (mb)	SD (mb)	T_{50} (years)	Periodicities (years) contributing to maximum normalized variance (H) in the waveband, with $H \geqslant 1{\cdot}0$						
W	−28	32	DJF	1013·1	1·2	3·8	2·1	2·7	3·2	4·0	5·3	10·1	21·8
			MAM	1017·0	0·7	3·9	2·6	2·9	3·7	4·7	5·9	7·9	12·9
			JJA	1021·8	1·3	7·8	2·0	2·4	3·3	5·7	7·8	23·4	
			SON	1017·7	1·0	7·2	2·5	3·4	4·8	7·1	10·3		
			ANN	1017·4	0·5	9·5	2·0	3·2	9·3				
X	−28	34	DJF	1013·1	1·1	3·5	2·7	3·3	4·3				
			MAM	1016·7	0·6	5·8	2·2	2·6	3·1	5·9	9·5		
			JJA	1021·9	1·3	3·4	2·2	2·4	2·7	3·5	4·8	19·7	
			SON	1017·4	1·0	4·3	2·2	2·9	3·6	4·7	20·6		
			ANN	1017·3	0·7	4·4	2·1	2·7	3·3	20·8			
Y	−30	114	DJF	1011·3	1·2	4·3	2·9	3·6	4·6	22·8			
			MAM	1015·5	1·5	4·0	2·5	2·9	3·5	21·4			
			JJA	1018·0	1·7	3·6	2·7	3·5	8·1	14·8			
			SON	1016·1	1·3	3·1	2·1	2·4	3·0	3·8	5·1	18·8	
			ANN	1015·2	0·9	4·6	3·5	5·3	19·2				
Z	−32	110	DJF	1014·8	1·1	3·2	2·6	4·7	5·9	8·1	23·9		
			MAM	1017·5	1·5	3·3	2·1	2·5	3·4	5·4			
			JJA	1018·4	1·8	3·5	2·1	2·7	3·3	4·9	13·3		
			SON	1018·2	1·2	4·6	2·5	3·5	4·4	13·5			
			ANN	1017·2	0·9	3·6	2·1	3·4	4·2	5·3	14·4		

* Time series does not follow normal distribution characteristics.

Table II. Periodogram estimates (percentages of total number of grids)—COADS seasonal (September–November) mean surface pressure 1961–1988

	Total number of grids	Data normal distribution	Var spec normal distribution	$t_{50} \leqslant 5{\cdot}5$ (years)	Dominant (normalized var > 1) peak periodicities in wavebands (years)					
					2–3	3–4	4–8	8–12	12–20	20–28
Northern Hemisphere	1590	94	89	85	97	96	91	43	42	13
Southern Hemisphere	153	97	95	93	95	67	97	29	42	25

total variance; (iii) the periodicities contributing maximum normalized variance in wavebands with normalized variance equal to or exceeding 1. Almost all the surface pressure data series used in this study are found to exhibit normal distribution characteristics except for a few marked by asterisks in Table I.

Table II gives periodogram estimates similar in content to Table I for all available grid-points in the Northern and Southern Hemispheres for one representative season (September to November) for the same period of study.

DISCUSSION AND CONCLUSION

From Figures 1–5 and Table II it is seen that the spectra of temporal (years) fluctuations of atmospheric surface pressure follows the universal and unique inverse power law form of the statistical normal distribution such that the square of the eddy amplitude represents the eddy probability density corresponding to the normalized standard deviation t equal to $[(\log L_m/\log T_{50}) - 1]$, where L_m is the period in years and T_{50} refers to the period up to which the cumulative percentage contribution to total variance is equal to 50. Inverse power law form for the power

spectra of temporal fluctuations is a signature of self-organized criticality in the non-linear variability of atmospheric surface pressure. The unique quantification for self-organized criticality in terms of the statistical normal distribution presented in this paper implies predictability of the total pattern of fluctuations in the atmospheric surface pressure over a period of time, 25 years in the present study. Universal spectrum rules out linear secular trends in atmospheric surface pressure.

The peak periodicities in the wavebands with normalized variance equal to or more than 1 (Tables I and II) correspond to the time periods of the internal circulations of the quasi-periodic Penrose tiling pattern and are, respectively, equal to $T(2 + \tau) = 3{\cdot}6T$, $T\tau(2 + \tau) = 5{\cdot}8T$, $T\tau^2(2 + \tau) = 9{\cdot}5T$, $T\tau^3(2 + \tau) = 15{\cdot}3T$, and $T\tau^4(2 + \tau) = 24{\cdot}8T$, where T, the primary perturbation time period, is the annual cycle of solar heating. The quasi-biennial oscillation (≈ 2 years), which is present in all the data sets analysed, may correspond to the period $T(2/\tau + 1) = 2{\cdot}2T$ of the small-scale circulation internal to the primary circulation according to the concept of the eddy continuum energy structure. The dominant periodicities in the atmospheric surface pressure time series therefore may be expressed as functions of the golden mean and these periodicities are intrinsic to atmospheric flows powered by the annual cycle of solar heating. The above model-predicted periodicities are found to occur frequently in meteorological data (instrumental and proxy) that includes North Atlantic pressure (Burroughs, 1992). Periodicities up to 5 years contribute as much as 50 per cent of the total variance and therefore near-future flow pattern trends may be estimated by the high-frequency periodicities up to 5 years. The present study shows that atmospheric flows self-organize to form a universal eddy continuum. Such a concept rules out indefinite linear trends in weather patterns. Enhanced energy input to the atmospheric eddy continuum due to anthropogenic greenhouse-gas-induced atmospheric warming will result in propagation of energy to all scales and intensification of weather systems of all scales. Such climate change may be seen immediately as an intensification of high-frequency fluctuations, such as QBO, ENSO, and smaller periodicities. The above model predictions are consistent with the following studies. Agee (1991) finds an increase in frequency of cyclone and anticyclone events for the Northern Hemisphere during periods of warming and a decrease during periods of cooling, as determined from NASA temperature for this century. Recent increases have been found in the intensity of the winter atmospheric circulation over the extratropical Pacific and Atlantic. These findings are reflected in an analysis of the climate of 1980 (IPCC, 1992).

ACKNOWLEDGEMENTS

The authors express their gratitude to Dr A.S.R. Murty for his keen interest and encouragement during the course of this study. Thanks are due to Mrs Arati A. Ursekar for typing this manuscript.

REFERENCES

Agee, E. M. 1991. 'Trends in cyclone and anticyclone frequency and comparison with periods of warming and cooling over the northern hemisphere', *J. Climate*, **4**, 263–267.

Agnew, D. C. 1992. 'The time domain behaviour of power-law noises', *Geophys. Res. Lett.*, **19**, 333–336.

Bak, P., Tang, C. and Wiesenfeld, K. 1988. 'Self-organized criticality', *Phys. Rev.*, **A38**, 364–374.

Bak, P. and Chen, K. 1989. 'The physics of fractals', *Physics D*, **38**, 5–12.

Barnett, T. P. 1991. 'The interaction of multiple time scales in the tropical climate system', *J. Climate*, **4**, 269–285.

Burroughs, W. J. 1992. *Weather Cycles: Real or Imaginary?*, Cambridge University Press, Cambridge, 197 pp.

Chao, Yi and Philander, S. G. 1993. 'On the structure of the Southern Oscillation', *J. Climate*, **6**, 450–469.

COADS 1985. *Comprehensive Ocean Atmosphere Data Set Release 1*, NOAA-ERL, Boulder, CO.

Goldberger, A. L., Rigney, D. R. and West, B. J. 1990. 'Chaos and fractals in human physiology', *Sci. Amer. (Ind. Edn.)*, **Feb.**, 40–47.

IPCC 1992. *Climate Change: The Supplementary Report to the IPCC Scientific Assessment*, Houghton, J. T., Callander, B. A. and Varney, S. K. (eds) Cambridge University Press, Cambridge, 200 pp.

Jean, R. V. 1994. *Phyllotaxis: a Systemic Study in Plant Morphogenesis*, Cambridge University Press, Cambridge, MA 376 pp.

Jenkinson, A. F. 1977. *A Powerful Elementary Method of Spectral Analysis for use with Monthly, Seasonal or Annual Meteorological Time Series*, Meteorological Office, London, Branch Memorandum No. 57, pp. 1–23.

Lamb, H. H. 1972. *Climate: Present, Past, Future*, Vol. I: *Fundamentals and Climate Now*, Methuen, London, 613 pp.

Lorenz, E. N. 1990. 'Can chaos and intransitivity lead to interannual variability?', *Tellus*, **42A**, 378–389.

Lovejoy, S. and Schertzer, D. 1986. 'Scale invariance, symmetries, fractal and stochastic simulations of atmospheric phenomena', *Bull. Am. Meteorol. Soc.*, **67**, 21–32.

Mandelbrot, B. B. 1977. *Fractals: Form, Chance and Dimension*, W. H. Freeman, San Francisco, 365 pp.

Mary Selvam, A. 1990. 'Deterministic chaos, fractals and quantumlike mechanics in atmospheric flows', *Can. J. Phys.*, **68**, 831–841.

Mary Selvam, A. 1993a. 'Universal quantification for deterministic chaos in dynamical systems', *Appl. Math. Model.*, **17**, 642–649.
Mary Selvam, A. 1993b. 'A universal spectrum for interannual variability of monsoon rainfall over India', *Adv. Atmos. Sci.*, **10**(2), 221–226.
Mary Selvam, A., Pethkar, J. S. and Kulkarni, M. K. 1992. 'Signatures of a universal spectrum for atmospheric inter-annual variability in rainfall time series over the Indian region', *Int. J. Climatol.*, **12**, 137–152.
Philander, S. G. 1990. *El Niño, La Niña and the Southern Oscillation*, Academic Press, NY, International Geophysical Series 46, 291 pp.
Schroeder, M. 1991. *Fractals, Chaos and Power Laws*, W.H. Freeman, San Francisco, 417 pp.
Selvam, A. M. and Joshi, R. R. 1995. 'Universal spectrum for interannual variability in COADS global air and sea surface temperatures', *Int. J. Climatol.*, **15**, 613–624.
Selvam, A. M. and Radhamani, M. 1994. 'Signatures of a universal spectrum for nonlinear variability in daily columnar total ozone content', *Adv. Atmos. Sci.*, **11**(3), 335–342.
Skinner, J. E. 1994. 'Low-dimensional chaos in biological systems', *Biotechnology*, **12**, 596–600.
Spiegel, M. R. 1961. *Statistics*, McGraw-Hill, NY, 359 pp.
Stewart, I. 1995. 'Daisy, daisy, give me your answer, do', *Sci. Am.*, ***Jan.***, 76–79.
Tessier, Y., Lovejoy, S. and Schertzer, D. 1993. 'Universal multifractals: theory and observations for rain and clouds', *J. Appl. Meteorol.*, **32**, 223–250.
Townsend, A. A. 1956. *The Structure of Turbulent Shear Flow*, Cambridge University Press, Cambridge, 130 pp.
Tsonis, A. A. and Elsner, J. B. 1990. 'Multiple attractors, fractal basins and long-term climate dynamics', *Beitr. Phys. Atmosph.*, **63**, 171–176.
West, B. J. 1990. 'Physiology in fractal dimensions', *Ann. Biomed. Eng.*, **18**, 135–149.
West, B. J. and Shlesinger, M. F. 1989. 'On the ubiquity of 1/*f* noise', *Int. J. Mod. Phys. B.*, **3**(6), 795–819.